SCIENCE CHINA
Information Sciences

• RESEARCH PAPER •

August 2021, Vol. 64 182312:1–182312:10
https://doi.org/10.1007/s11432-020-3025-4

Theoretical analysis of PAM-N and M-QAM BER computation with single-sideband signal

Dongxu LU[1], Xian ZHOU[1,2*], Yuqiang YANG[1], Jiahao HUO[1,2], Jinhui YUAN[1,2], Keping LONG[1], Changyuan YU[1,2], Alan Pak Tao LAU[3] & Chao LU[2]

[1]*Beijing Engineering and Technology Research Center for Convergence Networks and Ubiquitous Services, University of Science and Technology Beijing, Beijing* 100083*, China;*
[2]*Department of Electronic and Information Engineering, The Hong Kong Polytechnic University, Hong Kong* 999077*, China;*
[3]*Department of Electrical Engineering, The Hong Kong Polytechnic University, Hong Kong* 999077*, China*

Received 14 January 2020/Revised 29 March 2020/Accepted 31 July 2020/Published online 2 June 2021

Abstract In this paper, the theoretical bit error rate (BER) of N-level pulse amplitude modulation (PAM-N) and M-ary quadrature amplitude modulation (M-QAM) have been studied and compared under different scenarios, including (i) PAM with intensity modulation with direct detection (IM/DD) and field modulation with detection (FMD) (including coherent detection and single-sideband modulation with direct detection (SSB-DD)), and (ii) QAM with coherent detection and SSB-DD. Considering the relationship between the symbol spacing and signal-to-noise ratio (SNR), we provide the mathematical BER equations, including the optical signal-to-noise ratio (OSNR) and carrier-to-signal power ratio (CSPR), especially for PAM signals. To verify the validity of our theoretical expressions for SSB systems, transmissions with 224-Gb/s SSB-PAM4/16QAM signals using the Kramers-Kronig (KK) receiver were implemented on a unified optical system platform. The simulation results agreed well with theoretical calculations both in back-to-back (BtB) and 120-km transmission scenarios, which showed that the BER evaluation methods can serve as a theoretical guidance and system assessment criteria for SSB scenarios.

Keywords N-level pulse amplitude modulation (PAM-N), M-ary quadrature amplitude modulation (M-QAM), BER computation, single-sideband (SSB), Kramers-Kronig receiver

Citation Lu D X, Zhou X, Yang Y Q, et al. Theoretical analysis of PAM-N and M-QAM BER computation with single-sideband signal. Sci China Inf Sci, 2021, 64(8): 182312, https://doi.org/10.1007/s11432-020-3025-4

1 Introduction

The recent decade has shown considerable development of high-capacity data center interconnects (DCI) [1]. In these short-reach scenarios, single-sideband (SSB) modulation has become a very promising scheme because it can overcome the inherent chromatic dispersion-induced power fading effect. For example, in [2], a novel non-optical carrier single-sideband orthogonal frequency division multiplexing (NOC-SSB-OFDM) scheme was proposed for intensity modulation and heterodyne detection-based passive optical networks (PONs). Among these, SSB with pulse amplitude modulation (PAM) and quadrature amplitude modulation (QAM) have been considered as the two most commonly used modulation formats owing to the simplicity and flexibility of digital coding [3–7]. Moreover, it is possible to recover the full electric field by using a Kramers-Kronig (KK) receiver, where the carrier-to-signal power ratio (CSPR) is considered a crucial parameter for achieving a balance between the minimum phase condition and optical signal-to-noise ratio (OSNR) [8–10]. As studied in [6], a 224-Gb/s Nyquist 16-ary quadrature amplitude modulation (16-QAM) signal over a 75-km standard single-mode fiber (SSMF) with a bit error rate (BER) of less than 3.8×10^{-3} in a single-sideband modulation with direct detection (SSB-DD) system

* Corresponding author (email: zhouxian219@ustb.edu.cn)

using digital CD pre-management and a KK receiver was successfully demonstrated via numerical simulations. Additionally, several studies have been reported in the computation of BER and signal-to-noise ratio (SNR) for some cases [11–15]. In [11, 12], based on signal-space concepts, mathematical expressions were derived and were used to compute the BER of M-QAM efficiently and accurately. In [13–15], the BER equations for N-level PAM (PAM-N) with intensity modulation with direct detection (IM/DD) were given in terms of the probability distribution characteristics for the Gaussian noise-limited scenarios. However, it is difficult to evaluate and compare the performance fairly for different scenarios without a theoretical reference. Moreover, in contrast to IM/DD, the electric field information of the signal can be detected in certain scenarios, which are defined as the field modulation with detection (FMD) in this paper. In FMD scenarios, the signals with a zero mean value can be detected by coherent detection or SSB-DD methods. Thus, the coherent detection with carrier suppression can be regarded as the basic FMD mode, and SSB-DD is categorized as a kind of FMD with an additional carrier. Based on this, the theoretical BER computations of QAM and PAM in the coherent detection and SSB-DD scenarios have been reorganized, as shown in Section 2.

In this study, theoretical BER computations of N-level (PAM-N) and M-ary quadrature amplitude modulation (M-QAM) were investigated and were summarized for different scenarios, which include (i) PAM with IM/DD and FMD (including coherent detection and SSB-DD) and (ii) QAM with FMD (including coherent detection and SSB-DD). To verify the theoretical analysis, the transmissions of DD systems with 224-Gb/s SSB-PAM4/16QAM were implemented, where the influences of the CSPR and OSNR on the system performance were shown and analyzed. The results showed that the theoretical analyses are consistent with the simulation results, which can provide theoretical guidance and system evaluation criteria to achieve optimum performance for SSB scenarios. Moreover, an impressive conclusion was drawn from this study: if under the same bit rates, CSPRs, and OSNRs, the BER performances of PAM-4 and 16-QAM should be equivalent.

2 Theoretical analysis of PAM-N and M-QAM BER computation

First, to acquire the theoretical relationship between the BER and OSNR in optical systems, the derivation of the SNR_b (E_b/N_0) and OSNR is given by [4]

$$\mathrm{OSNR} = \frac{P_{\mathrm{Signal}}}{P_{\mathrm{Noise}}} = \frac{E_b R_b}{2B_{\mathrm{ref}} N_0} = \frac{R_b}{2B_{\mathrm{ref}}} \cdot \mathrm{SNR}_b, \tag{1}$$

where E_b denotes the signal average energy per bit and N_0 is the spectrum density of the amplified spontaneous emission (ASE) noise in one polarization. R_b refers to the total bit rate of system. In particular, B_{ref} is the optical bandwidth reference set as 0.1 nm, corresponding to the value of 12.5 GHz. Besides, the noise considered in this paper is zero mean additive white Gaussian noise (AWGN) with the variance of $N_0/2$.

2.1 Theoretical analysis of PAM-N

The conclusion of the generalized expression for the BER computation of a PAM-N signal in IM/DD systems can be found in [15], which is given by

$$\begin{aligned}\mathrm{BER}_{\mathrm{PAM}} &= \frac{1}{\log_2(N)} \sum_{i=1}^{N} P(I_i)(P(I_{i-1}\,|I_i) + P(I_{i+1}\,|I_i)) \\ &= \frac{1}{N\log_2(N)} \sum_{i=1}^{N} (P(I_{i-1}\,|I_i) + P(I_{i+1}\,|I_i)),\end{aligned} \tag{2}$$

where N is the PAM level, I_i is the ith electrical level of symbol, $P(I_i)$ is the probability of transmitting symbol I_i and $P(I_{i-1}|I_i)$ or $P(I_{i+1}|I_i)$ denotes the probability of deciding I_{i-1} or I_{i+1} when I_i is transmitted, respectively. As all symbols are equally probability transmitted, it can be deduced that $P(I_i) = 1/N, \forall i$. Assuming Gray coding is adopted, wrong symbol decisions can only be made to either one of the two closest neighboring symbols [15]. For the first and last symbols I_1 and I_N, erroneous symbol level decision can only be made on one side and $P(I_0\,|I_1) = P(I_{N+1}\,|I_N) = 0$. We also assume

that the decision thresholds are equidistant from adjacent symbols. Besides, the relation between BER and symbol error rate (SER) should be BER = $\frac{1}{\log_2(N)}$SER. To give an accurate relation of BER computing for PAM-N signal, a detailed and simplified derivation using mathematical characteristics of noise distribution is found to be

$$\begin{aligned}\mathrm{BER}_{\mathrm{PAM}} &= \frac{2(N-1)}{N\log_2(N)}P(I_{i-1}\,|I_i) = \frac{2(N-1)}{N\log_2(N)}P\left(Z < \frac{I_{\mathrm{i}-1}-I_i}{2}\right)\\ &= \frac{N-1}{N\log_2(N)}\mathrm{erfc}\left(\frac{d}{2\sqrt{2}\sigma}\right),\end{aligned} \tag{3}$$

where Z represents the AWGN and d is the distance between the two adjacent symbols. Considering the symmetry of Gaussian distribution, it can be concluded that $P(I_i|I_{i-1}) = P(I_{i-1}|I_i) = P(I_{i+1}|I_i) = P(I_i|I_{i+1})$ and $\sum_{n=1}^{N}(P(I_{i-1}|I_i) + P(I_{i+1}|I_i)) = 2(N-1)P(I_{i-1}|I_i)$. The symbol I_i can be wrongly decided to I_{i-1} when $I_i + Z < \frac{I_{i-1}+I_i}{2}$, that is, $Z < \frac{I_{i-1}-I_i}{2}$. In the following subsections, the scenarios of the PAM signals with IM/DD and FMD (coherent detection and SSB-DD) are analyzed using the theory of BER computation with OSNR and CSPR.

2.1.1 *PAM with IM/DD*

In this situation, the electrical levels of PAM signal ($s(t)$) are distributed from 0 to $(N-1)l$, where l represents the unit electrical level and $d = l$. $\sqrt{s(t)}$ represents the signal after the intensity modulation. After square-law detection, the photocurrent $r(t)$ is proportional to $|\sqrt{s(t)}|^2$. Thus, the whole IM/DD process can be described by

$$r(t) \propto \left|\sqrt{s(t)}\right|^2, \quad s(t) \geqslant 0, \tag{4}$$

where the values of $s(t)$ are limited to be non-negative. Thus, the relation between d and E_b can be acquired by calculating the average power per symbol of the signal (E_s), which is given by

$$E_s = \log_2 N \cdot E_b = \frac{1^2+2^2+3^2+\cdots+(N-1)^2}{N}l^2, \quad l = d = \sqrt{\frac{6\log_2 N \cdot E_b}{(N-1)(2N-1)}}. \tag{5}$$

Combining (1), (3) and (5), the theoretical expression between the BER and OSNR in IM/DD situation can be given by

$$\begin{aligned}\mathrm{BER}_{\text{IMDD-PAM}} &= \frac{N-1}{N\log_2(N)}\mathrm{erfc}\left(\sqrt{\frac{3\log_2(N)}{2(N-1)(2N-1)}\cdot\frac{E_b}{N_0}}\right)\\ &= \frac{N-1}{N\log_2(N)}\mathrm{erfc}\left(\sqrt{\frac{3\log_2(N)}{2(N-1)(2N-1)}\cdot\frac{2B_{\mathrm{ref}}}{R_b}}\cdot\sqrt{\mathrm{OSNR}}\right).\end{aligned} \tag{6}$$

To demonstrate more directly, based on (6), Figure 1 shows the system performance of PAM-N signals with different N-levels (i.e., 2, 4, 6, ..., 16) at the same bit rate of 224-Gb/s. It can be seen from Figure 1, that higher-order PAM signals require higher OSNR under the same BER floor and can be more sensitive to channel impairments such as CD. For example, at the BER threshold of 7% forward-error-correction (FEC), the PAM-4 signals require 5 dB more OSNR than PAM-2 in IM/DD systems.

2.1.2 *PAM with FMD*

(1) Coherent detection systems. In this paper, the coherent detection systems with carrier suppression are regarded as the basic FMD systems. The electrical levels of the transmitted signals are distributed symmetrically around zero, i.e., $-(N-1)l, -(N-3)l, \ldots, -l, l, \ldots, (N-1)l$ with $d = 2l$. In this situation, the photocurrent $r(t)$ is proportional to transmitted signal $s(t)$ and the process of coherent detection can be described by

$$r(t) \propto s(t), \quad \overline{s(t)} = 0, \tag{7}$$

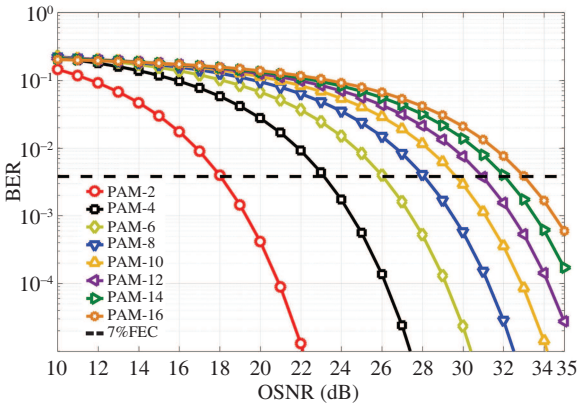

Figure 1 (Color online) Theoretical BER vs. OSNR for 224-Gb/s PAM-N signals in IM/DD case.

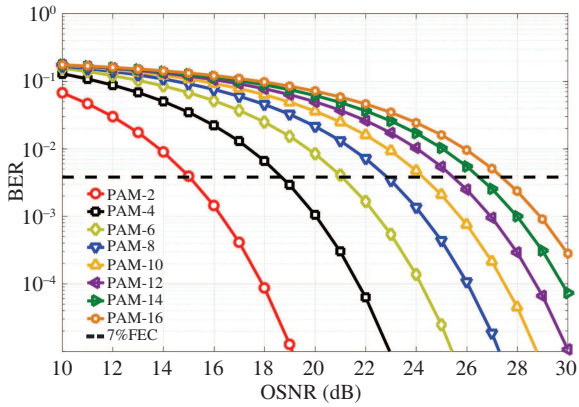

Figure 2 (Color online) Theoretical BER vs. OSNR for 224-Gb/s PAM-N signals in coherent detection case.

where $\overline{s(t)}$ represents the mean value of signal. For FMD scenarios, the transmitted signals can be positive or negative and detected by coherent detection or SSB-DD approaches. Thus, the relation between d and E_b can be expressed by

$$E_s = \log_2 N \cdot E_b = \frac{2(1^2 + 3^2 + \cdots + (N-1)^2)}{N} l^2, \quad l = \frac{d}{2} = \sqrt{\frac{3\log_2 N \cdot E_b}{(N+1)(N-1)}}. \tag{8}$$

Therefore, the theoretical relationship between the OSNR and BER in coherent detection systems can be acquired by combining (1), (3) and (8):

$$\mathrm{BER}_{\text{CO-PAM}} = \frac{N-1}{N\log_2(N)} \mathrm{erfc}\left[\sqrt{\frac{3\log_2(N)}{(N+1)(N-1)} \cdot \frac{2B_{\text{ref}}}{R_b}} \sqrt{\mathrm{OSNR}}\right]. \tag{9}$$

Similarly, Figure 2 is conducted based on (9) and as shown here, all the OSNRs required at the same BER floors in coherent detection are lower than the IM/DD. This is because the distribution of signals with coherent detection occupies the full linear modulation region, compared with only the positive part in IM/DD case. For example, the PAM-4 signal with coherent detection requires 4 dB more OSNR than that with IM/DD at the 7% FEC threshold.

(2) SSB-DD systems. Although using the square-law detection of one single photodetector (PD), the SSB-DD systems can preserve the complete electric field information owing to the existence of the strong carrier. The optical carrier in SSB-DD systems is analogous to the local oscillators (LO) in conventional coherent optical schemes. In fact, the SSB-DD system is a kind of heterodyne system essentially. In this paper, the SSB-DD systems are regarded as a kind of FMD systems with the carrier component (A) added. After the PD detection, DC-removal and SSBI cancellation, the photocurrent $r(t)$ can be described as

$$r(t) \propto \left|A + s(t) \cdot \mathrm{e}^{\mathrm{j}2\pi f_b t}\right|^2 \approx A \cdot s(t) \mathrm{e}^{\mathrm{j}2\pi f_b t}, \quad \overline{s(t)} = 0, \tag{10}$$

where f_b is the frequency offset of SSB signals. In SSB-DD systems, the effect of carrier power should be considered in the theoretical relationship between BER and OSNR. For clarity, the OSNR_m represents the measured OSNR with the carrier included in the signal, and the OSNR indicates no carrier included in the signal, called the equivalent OSNR in this paper. Based on these definitions, the relation between the OSNR_m, OSNR and CSPR is given by

$$\mathrm{OSNR}_m = \frac{P_{\text{signal}} + P_{\text{carrier}}}{P_{\text{noise}}} = \frac{P_{\text{signal}}}{P_{\text{noise}}} \left(1 + \frac{P_{\text{carrier}}}{P_{\text{signal}}}\right) = \mathrm{OSNR} \cdot (1 + \mathrm{CSPR}). \tag{11}$$

Substituting (11) into (9), a certain numerical conclusion of the BER, OSNR_m and CSPR in SSB-DD systems can be expressed by

$$\mathrm{BER}_{\text{SSB-PAM}} = \frac{N-1}{N\log_2(N)} \mathrm{erfc}\left[\sqrt{\frac{3\log_2 N}{(N+1)(N-1)} \cdot \frac{2B_{\text{ref}}}{R_b}} \sqrt{\frac{\mathrm{OSNR}_m}{\mathrm{CSPR}+1}}\right]. \tag{12}$$

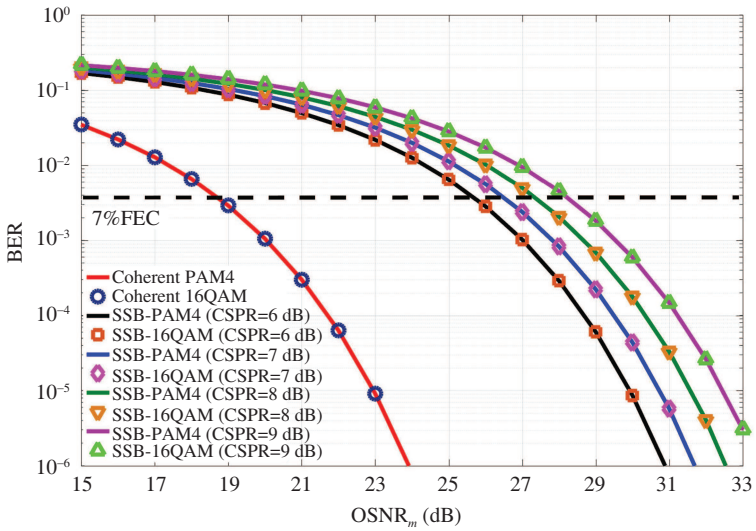

Figure 3 (Color online) Theoretical BER vs. OSNR$_m$ for 224-Gb/s PAM-4 and 16-QAM signals in coherent detection and SSB-DD cases at different CSPRs.

2.2 Theoretical analysis of M-QAM

The QAM signal can be detected by coherent detection or SSB-DD approaches, which are both the FMD mode. The BER expression of M-QAM modulation in coherent detection (namely basic FMD) scenarios can be given by [11]

$$\begin{aligned}\mathrm{BER}_{\text{CO-QAM}} &= \frac{2(\sqrt{M}-1)}{\sqrt{M}\log_2 M}\mathrm{erfc}\left(\sqrt{\frac{3\log_2 M}{2(M-1)}\cdot\frac{E_b}{N_0}}\right)\\ &= \frac{2(\sqrt{M}-1)}{\sqrt{M}\log_2 M}\mathrm{erfc}\left(\sqrt{\frac{3\log_2 M}{2(M-1)}\cdot\frac{2B_{\text{ref}}}{R_{\text{b}}}\cdot\mathrm{OSNR}}\right).\end{aligned} \tag{13}$$

Thus, we can also acquire the BER computing of QAM with SSB-DD by substituting (11) into (13), that is

$$\mathrm{BER}_{\text{SSB-QAM}} = \frac{2(\sqrt{M}-1)}{\sqrt{M}\log_2 M}\mathrm{erfc}\left(\sqrt{\frac{3\log_2 M}{2(M-1)}\cdot\frac{2B_{\text{ref}}}{R_{\text{b}}}}\cdot\sqrt{\frac{\mathrm{OSNR}_m}{\mathrm{CSPR}+1}}\right). \tag{14}$$

2.3 Theoretical relation between PAM-4 and 16-QAM

By comparing (9) and (13), (12) and (14), a theoretical relationship between PAM-4 and 16-QAM in coherent detection and SSB-DD scenes can be deduced,

$$\mathrm{BER}_{\text{CO-PAM4}} = \mathrm{BER}_{\text{CO-16QAM}} = \frac{3}{8}\mathrm{erfc}\left(\sqrt{\frac{6}{15}\cdot\frac{2B_{\text{ref}}}{R_b}}\sqrt{\mathrm{OSNR}}\right), \tag{15}$$

$$\mathrm{BER}_{\text{SSB-PAM4}} = \mathrm{BER}_{\text{SSB-16QAM}} = \frac{3}{8}\mathrm{erfc}\left(\sqrt{\frac{6}{15}\cdot\frac{2B_{\text{ref}}}{R_b}}\cdot\sqrt{\frac{\mathrm{OSNR}_m}{\mathrm{CSPR}+1}}\right). \tag{16}$$

Here, we can conclude that PAM-4 signals share the same BER computing formula with 16-QAM in coherent detection, which is also applicable in SSB-DD scenarios. Thus, under the same CSPRs and bit rates, the curves of the OSNR$_m$ versus BER in the two scenarios with PAM-4 and 16-QAM should coincide perfectly, which is also verified in Figure 3. For clarity, Table 1 is summarized to show that the PAM/QAM signals with different modulation can be detected by different detection methods and referred to different BER formulas in these situations.

Table 1 Comparison of different modulation and detection methods for PAM and QAM

Format	Modulation and detection methods		Eq.
PAM	IM/DD: 0 1 2 3		(6)
	FMD: ... −3 −1 1 3 ...	Coherent detection	(9)
		SSB-DD	(12)
QAM	FMD: 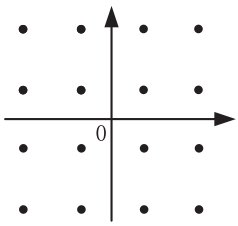	Coherent detection	(13)
		SSB-DD	(14)

Figure 4 (Color online) Simulation setup and DSP block diagram of SSB PAM-4/16-QAM systems.

Table 2 General simulation parameters of 224-Gbit/s SSB-DD systems

Parameter	Value	Unit
Bit rate	224	Gbit/s
DAC/ADC sampling rate	112	GSa/s
ENOB of DAC/ADC	6	bits
Laser central frequency (f_c)	193.1	THz
Laser linewidth (laser1&laser2)	100	kHz
V_π (IQM&DDMZM)	15	dBm
Extinction ratio (IQM)	30	dB
Fiber length	120	km
Chromatic dispersion	17	ps/nm/km
PD responsibility	0.65	A/W
PD thermal noise	20	pA/Hz$^{0.5}$
PD dark current	10	nA

3 Simulation setup

To verify the validity of the theoretical equations for SSB-DD systems, as mentioned in Section 2, Figure 4 shows the simulation setup and DSP block diagram, and the key simulation parameters are summarized in Table 2. This was conducted using VPItransmissionMaker and Matlab.

First, a pseudorandom binary sequence (length = $2^{16}-1$) was mapped onto the PAM/QAM symbols.

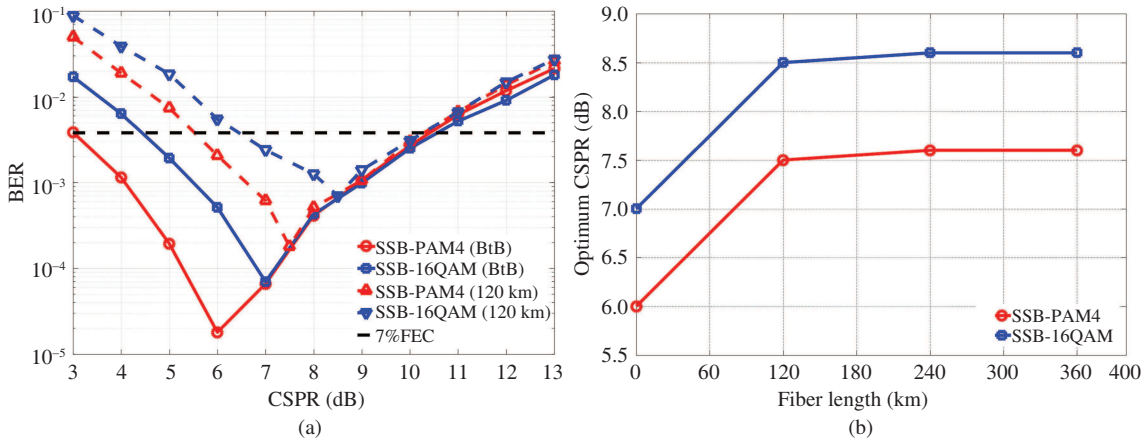

Figure 5 (Color online) (a) BER performances as a function of the CSPR for 112-Gbaud SSB-PAM4 and 56-Gbaud SSB-16QAM with KK method in the BTB and 120-km transmission scenarios, (b) the required optimum CSPR as a function of the SSMF transmission length.

The symbols were up-sampled and passed through a root-raised-cosine (RRC) filter for Nyquist pulse shaping with a roll-off factor of 0.01. Here, the SSB-PAM signal can be obtained by eliminating one sideband of the DSB-PAM by using a Hilbert filter, which does not need up-/down-conversion. In this study, in order to adjust the CSPR flexibly without considering additional modulation nonlinear effects, the optical carrier-assisted scheme was employed for both PAM/QAM systems and the IQ modulator was biased at its null-point [16]. As shown in Figure 4, laser2 was added as an additional optical carrier with a linewidth of 100 kHz (the same as laser1), and the two lasers were correlated by setting the same random seed number. In terms of linewidth effects, it was the same as in the modulation schemes of bias control using the IQ modulator or dual-drive Mach-Zehnder modulator (DDMZM). In this situation, the linewidth-induced phases of the signal and the carrier were kept the same, and after detection, the phase noise (PN) was cancelled out from each other. This made it unnecessary to adopt the phase recovery algorithm at the receiver [17]. However, if using two uncorrelated lasers, the linewidth compensation method should be considered [18]. Next, the central frequencies of the two lasers were both f_c for PAM, but for QAM, the frequencies of laser1 and laser2 were f_c and a 0.505×symbol rate ($f_s = 56$ GHz for 16-QAM) offset for f_c, respectively. Before launched into a 120-km SSMF link, the SSB signal was amplified by an erbium-doped fiber amplifier (EDFA) with an adjustable noise figure and a launch power of 1 mW to compensate the fiber loss. The fiber dispersion was 17 ps/nm/km, and the fiber nonlinearity was not considered. At the receiver, an optical band-pass filter (OBPF) was employed to remove the out-of-band noise. Then, the signal was detected by a single-ended PIN photodiode, followed by digitization using a single ADC. In the receiver DSP, the signal was initially resampled to four samples/symbol to tolerate the spectrum broadening caused by nonlinear operations in the KK scheme [19]. The desired PAM signal can be retrieved by real operation of the SSB-PAM signal after the CD compensation and equalization [17]. Additionally, the basedband QAM signal can be obtained by frequency down-conversion, followed by CD compensation, equalization, and the blind phase search (BPS) algorithm [20, 21]. For QAM signals, the BPS algorithm was used to eliminate the phase ambiguity induced by the constant modulus algorithm (CMA) adaptive equalization. Finally, the BER was calculated by error counting.

4 Results and discussion

The CSPR is a key parameter for SSB-based systems and it is certainly required to meet the minimum phase (MP) condition for KK detection. Before the MP condition is satisfied, the system performance will improve as the CSPR increases. However, when the MP condition is met, the performance will be degraded as the CSPR continues to increase. In this situation, the carrier power occupies most of the power component compared to the signal, and the equivalent OSNR is decreased when the total OSNR_m is fixed. Thus, there will be an optimum CSPR for the system. In this study, the CSPRs for the two SSB systems were first optimized in back-to-back (BtB) and 120-km transmission scenarios, as shown in Figure 5(a).

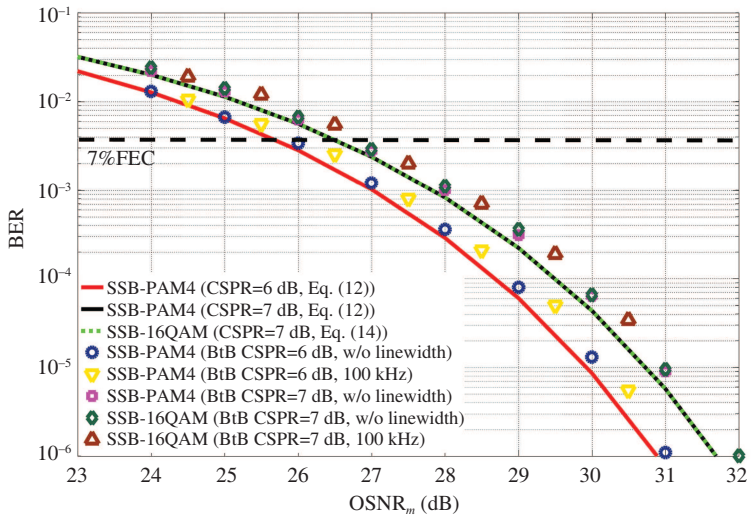

Figure 6 (Color online) Theoretical and simulated BER performances as a function of the OSNR$_m$ for 112-Gbaud SSB-PAM4 and 56-Gbaud SSB-16QAM with the optimized CSPRs in BtB scenario.

At a fixed OSNR$_m$ of 30 dB, the optimum CSPRs for the SSB-PAM4 and SSB-16QAM signals were 6 dB and 7 dB in the BtB case and 7.5 dB and 8.5 dB after a 120-km transmission, respectively. The SSB systems employing the KK algorithm both require 1.5 dB more CSPR than that of the BtB scenario after 120-km transmission. The main reason for this is that the CD effect induces an increase in the peak to average power ratio (PAPR) of the signal after fiber transmission, according to [22]. With a higher PAPR, the time trajectory of signals is more likely to encircle the origin of the complex plane, which will violate the MP condition [13, 14]. In this case, the KK algorithm needs a larger CSPR to satisfy the MP condition compared to the BtB case. Moreover, the difference in the optimum CSPRs between PAM-4 and 16-QAM is mostly because the 16-QAM signal requires a larger carrier than PAM-4 to guarantee the signal trajectory does not encircle the origin. Figure 5(b) shows the optimum CSPRs after the SSMF transmission of different lengths. After 120-km transmission, the PAPR of the signal induced by CD effects will tend to be stable; thus, the optimum CSPRs will remain at steady values [22].

To confirm the conclusion of BER computing described in Section 2, both the theoretical and simulation results with/without the laser linewidth in the BtB case were obtained, as shown in Figure 6. Here, the optimum CSPR of 6 dB was chosen for the SSB-PAM4 system, and 7 dB was chosen for the SSB-16QAM system. According to (16), under the same bit rates, CSPRs, and OSNRs, the BER performance of PAM-4 and 16-QAM should be equivalent. Thus, as shown in Figure 6, the theoretical curves for PAM-4 and 16-QAM coincide perfectly at a CSPR of 7 dB (black line and green dotted line). Based on the theoretical curves, the OSNR penalties between the theory and simulation at the 7% FEC threshold of 3.8×10^{-3} could be calculated, which was 0.1 dB for SSB-PAM4 at a CSPR of 6 dB (red line and dark blue circle), 0.1 dB for SSB-PAM4 at a CSPR of 7 dB (dark line and pink square) and 0.15 dB for SSB-16QAM at a CSPR of 7 dB (green dotted line and dark green diamond). Therefore, the small gaps between theory and simulation confirm the accuracy of (12) and (14). Moreover, the results for the 100-kHz linewidth using the two related lasers are also shown in Figure 6, which show the same system performance as in the case of bias control.

After a transmission distance of 120 km, the OSNR curves for SSB-PAM4 and SSB-16QAM were scanned, as shown in Figure 7, which was conducted under the optimized CSPRs of 7.5 dB and 8.5 dB, respectively. Without considering the linewidth, the theoretical and simulation results for PAM and QAM were also in good agreement: (i) the OSNR penalty at the 7% FEC BER threshold was 0.1 dB for SSB-PAM4 at a CSPR of 7.5 dB (red line and dark blue circle), (ii) 0.2 dB for SSB-PAM4 at a CSPR of 8.5 dB (the dark line and pink square) and 0.25 dB for SSB-16QAM at a CSPR of 8.5 dB (green dotted line and dark green diamond). From a comparison and analysis of the above results, the theoretical expressions of (12) and (14) can serve as evaluation criteria to provide confirmation of the SSB-DD system performance in both BtB and optical transmission scenarios. Additionally, unlike the BtB case, after a 120-km transmission, the OSNR penalties with 100-kHz linewidth at the 7% FEC threshold were 0.7 dB for SSB-PAM4 and 0.9 dB for SSB-16QAM compared with the case of no linewidth. This was mainly

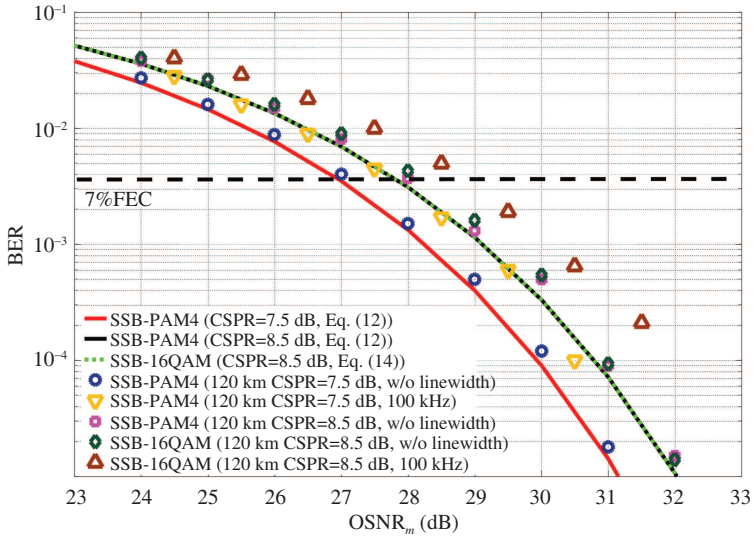

Figure 7 (Color online) Theoretical and simulated BER performances as a function of the OSNR$_m$ for 112-Gbaud SSB-PAM4 and 56-Gbaud SSB-16QAM with the optimized CSPRs after a 120-km transmission.

because the laser linewidth can interact with the dispersion to produce equalization-enhanced phase noise (EEPN) and phase to amplitude (P2A) noise, which will induce an additional OSNR penalty [23, 24].

5 Conclusion

In this paper, the theoretical analyses of BER computing and calculation formulas of PAM with IM/DD and FMD (coherent and SSB-DD), and QAM with FMD have been given in detail to investigate the inner link between BER, OSNR and CSPR. To verify these, the transmissions with 224-Gb/s SSB-PAM4/16QAM have been implemented. As a result, the theoretical conclusion is in good agreement with the results of numerical simulation both in BtB and optical transmission situations. Without considering the influence of linewidth, in BtB case, the deviations of OSNR penalty at the 7% FEC threshold are only 0.1 dB for SSB-PAM4 and 0.15 dB for SSB-16QAM between the theory and simulation under their each best CSPRs, and after a 120-km transmission, the gaps are 0.1 dB and 0.25 dB, respectively. This paper can offer a theoretical basis and assessment criteria of system optimization and evaluation, which will be helpful to guide the design of experimental work.

Acknowledgements This work was supported by National Key Research and Development Program of China (Grant No. 2019YFB1803905), National Natural Science Foundation of China (Grant Nos. 61871030, 61671053), Fundamental Research Funds for the Central Universities (Grant No. FRF-MP-19-009), State Key Laboratory of Advanced Optical Communication Systems Networks, China, Open Fund of IPOC (BUPT) (Grant No. IPOC2018B009), and Foundation of Beijing Engineering and Technology Center for Convergence Networks and Ubiquitous Services.

References

1 Zhong K P, Zhou X, Huo J H, et al. Digital signal processing for short-reach optical communications: a review of current technologies and future trends. J Lightwave Technol, 2018, 36: 377–400
2 Zhang X L, Zhang C F, Chen C, et al. Non-optical carrier SSB-OFDM PONs with the improved receiver sensitivity and potential transmission nonlinearity tolerance. IEEE Photonics J, 2017, 9: 1–10
3 Zhu M Y, Zhang J, Yi X W, et al. Optical single side-band Nyquist PAM-4 transmission using dual-drive MZM modulation and direct detection. Opt Express, 2018, 26: 6629–6638
4 Zhu Y X, Zou K H, Chen Z Y, et al. 224 Gb/s optical carrier-assisted Nyquist 16-QAM half-cycle single-sideband direct detection transmission over 160 km SSMF. J Lightwave Technol, 2017, 35: 1557–1565
5 Le S T, Schuh K, Chagnon M, et al. 1.72-Tb/s virtual-carrier-assisted direct-detection transmission over 200 km. J Lightwave Technol, 2018, 36: 1347–1353
6 Zhang X L, Zhang C F, Chen C, et al. Digital chromatic dispersion pre-management for SSB modulation direct-detection optical transmission systems. Optics Commun, 2018, 427: 551–556
7 Li A, Peng W-R, Cui Y, et al. 112 GBd virtual-carrier assisted single-sideband PAM4 with Kramers-Kronig detection and blind adaptive IQ imbalance compensation. In: Proceedings of Optical Fiber Communication Conference, 2019. 5
8 Mecozzi A, Antonelli C, Shtaif M. Kramers-Kronig coherent receiver. Optica, 2016, 3: 1220–1227
9 Mecozzi A. A necessary and sufficient condition for minimum phase and implications for phase retrieval. 2016. ArXiv:1606.04861
10 Li Z, Erkilinc M S, Shi K, et al. SSBI mitigation and the Kramers-Kronig scheme in single-sideband direct-detection transmission with receiver-based electronic dispersion compensation. J Lightwave Technol, 2017, 35: 1887–1893

11 Lu J H, Letaief K B, Chuang J C I, et al. M-PSK and M-QAM BER computation using signal-space concepts. IEEE Trans Commun, 1999, 47: 181–184
12 Yang L-L, Hanzo L. A recursive algorithm for the error probability evaluation of M-QAM. IEEE Commun Lett, 2000, 4: 304–306
13 Szczerba K, Westbergh P, Karout J, et al. 4-PAM for high-speed short-range optical communications. J Opt Commun Netw, 2012, 4: 885–984
14 Szczerba K, Westbergh P, Agrell E, et al. Comparison of intersymbol interference power penalties for OOK and 4-PAM in short-range optical links. J Lightwave Technol, 2013, 31: 3525–3534
15 Chagnon M, Osman M, Poulin M, et al. Experimental study of 112 Gb/s short reach transmission employing PAM formats and SiP intensity modulator at 13 μm. Opt Express, 2014, 22: 21018
16 Lu D X, Lau A P T, Lu C, et al. Theoretical CSPR analysis and performance comparison for four single-sideband modulation schemes with Kramers-Kronig receiver. IEEE Access, 2019, 7: 166257–166267
17 Antonelli C, Mecozzi A, Shtaif M. Kramers-Kronig PAM transceiver and two-sided polarization-multiplexed Kramers-Kronig transceiver. J Lightwave Technol, 2018, 36: 468–475
18 Li X, Luo M, Li C, et al. Direct detection of pilot-assisted PAM-4 signals with large phase noise tolerance. Opt Lett, 2019, 44: 5457–5460
19 Bo T W, Kim H. Kramers-Kronig receiver without upsampling. In: Proceedings of Optical Fiber Communication Conference, 2018. 2
20 Zhou X, Lu C, Lau A P T, et al. Low-complexity carrier phase recovery for square M-QAM based on S-BPS algorithm. IEEE Photon Technol Lett, 2014, 26: 1863–1866
21 Zhou X, Zhong K P, Gao Y L, et al. Modulation-format-independent blind phase search algorithm for coherent optical square M-QAM systems. Opt Express, 2014, 22: 24044–24054
22 Sun C, Che D, Ji H L, et al. Study of chromatic dispersion impacts on Kramers-Kronig and SSBI iterative cancellation receiver. IEEE Photon Technol Lett, 2019, 31: 303–306
23 Zhu M Y, Zhang J, Huang X T, et al. Influence of EEPN and P2A noise with CD pre- and post-compensation in optical SSB transmission and Kramers-Kronig receiver system. Opt Express, 2019, 27: 19664
24 Le S T, Schuh K. Experimental verification of equalization enhanced phase noise in Kramers-Kronig transmissions. In: Proceedings of Optical Fiber Communication Conference, 2019. 2